Nonlinear Spectral Mixture Modeling to Estimate Water-Ice Abundance of Martian Regolith

Szilárd Gyalay[1,2], Eldar Z. Noe Dobrea[2,3], Kathryn Chu[2,4], Karly M. Pitman[5]

February 19, 2019

[1]Corresponding Author (sgyalay@ucsc.edu) University of California, Santa Cruz; 1156 High Street; Earth and Planetary Sciences, Room A232; Santa Cruz, CA 95060

[2]NASA Ames Research Center

[3]Planetary Science Institute

[4]University of California, Berkeley

[5]Space Science Institute

Abstract

We present a new technique to estimate the abundance of water-ice in the Martian permafrost using Phoenix Lander Surface Stereo Imager (SSI) multispectral data. Past work estimated this abundance by employing radiative transfer methods to model the spectra of ice and regolith mixtures using the optical constants of water-ice and a Martian-analogue soil. Our technique removed the uncertainty of using an analogue (or of estimating a regolith composition) by deriving the optical constants directly from observations of icy regolith acquired before and after sublimation of the ice at similar viewing geometries. Laboratory spectral measurements of known mixtures of water-ice and dry soil at controlled viewing geometries allowed us to constrain the uncertainty in our technique. We found that model fits across the observational uncertainty will contain the actual water-ice fraction. We then applied the technique to Phoenix SSI observations of Snow White trench and Dodo-Goldilocks trench. For the Snow White Trench we estimated water-ice abundances consistent with pore-fill in the near-surface ice, consistent with atmospheric diffusion. For the Dodo-Goldilocks Trench we estimate water-ice abundances larger than pore-fill would allow. These results have implications to our understanding of the history of water-ice on Mars and the role of the regolith at high latitudes as a reservoir of atmospheric H_2O.

Key Words: Ices; Mars; Spectroscopy

1 Introduction

One of the key goals of the Mars Exploration program is understanding the history and state of water on Mars. Although the past decade has seen significant advances in this field, important questions remain pertaining to the emplacement of water in the late Amazonian. In this context, the northern lowlands are particularly intriguing because significant amounts of ice may be shallowly buried at mid- to high-latitudes (*e.g.* [Boynton *et al.*, 2002, Mellon *et al.*, 2004, Mellon *et al.*, 2009, Diez *et al.*, 2008, Plaut *et al.*, 2009, Dundas *et al.*, 2014, Dundas *et al.*, 2018]).

Much of the Martian regolith's upper few meters are thought to be in diffusive equilibrium with the atmosphere, meaning water-ice would merely fill the pore-space between regolith grains [Mellon *et al.*, 2004], and therefore constrains the volume of ice that can be stored. Indeed, experiments by [Hudson *et al.*, 2009] and [Siegler *et al.*, 2012] demonstrate pore-fill from water vapor diffusion under Mars surface conditions. Porosity in the uppermost dessicated layer of the regolith was estimated to vary between 25-60% at the Viking landing sites [Moore *et al.*, 1987], and between 50-55% at the Phoenix landing site [Zent *et al.*, 2010]. Ice-abundances greater than pore-fill fraction would suggest another emplacement mechanism, such as the freezing of a body of surface water [Carr *et al.*, 1990], subsurface growth of an ice lens [Konrad *et al.*, 1993], snowfall [Mischna *et al.*, 2003, Noe Dobrea *et al.*, 2018], or buried pack ice [Prettyman *et al.*, 2004].

The Mars Phoenix lander provided an opportunity to compare ice emplacement models [Mellon *et al.*, 2004] and remote sensing observations of Martian ground ice [Boynton *et al.*, 2002, Diez *et al.*, 2008] to *in situ* measurements [Mellon *et al.*, 2009, Smith *et al.*, 2009, Cull *et al.*, 2010]. Observations from the Mars Orbiter Camera (MOC) and the High Resolution Imaging Science Experiment (HiRISE) suggest that Phoenix landed in a periglacial area with a subsurface rheology of ice-cemented regolith (as opposed to pure ice) on a depth scale of 10m [Mellon *et al.*, 2008]. [Putzig *et al.*, 2014] detected a radar reflector at depths of 15-66 m in Shallow Radar (SHARAD) data of Green Valley and suggested it to be the base of ground ice within the valley. [Noe Dobrea *et al.*, 2015] used HiRISE observations of crater ejecta to infer the presence of an incompetent layer (unable to form or retain ejecta boulders) about 40 to 70 meters in thickness that exhibited a rapid rate of crater degradation, and suggested this to be a layer of ice-cemented soil likely emplaced by repeated cycles of snowfall, sublimation, and lag formation.

Two different tonalities of ice were measured at the Phoenix landing site: one brighter (in Dodo-Goldilocks and Upper Cupboard trenches) and the other darker (in Snow White, Neverland, Pet Donkey, Ice Man, Burn Alive, and La Mancha trenches) [Mellon *et al.*, 2009, Smith *et al.*, 2009, Cull *et al.*, 2010]. A difference in properties between the two hint at different emplacement mechanisms, where the brighter ice is interpreted to be slab-ice, while the darker ice is thought to be pore-filling [Mellon *et al.*, 2009, Cull *et al.*, 2010]. [Cull *et al.*, 2010] estimated the abundance of water-ice in trenches dug by the Mars Phoenix lander by modeling the spectra of the icy regolith using the radiative transfer methods outlined in [Hapke, 2012] and references therein with optical constants for Mauna Kea palagonite [Clancy *et al.*, 1995] as a substitute for unknown Martian regolith optical constants.

In this work we also used radiative transfer analysis to estimate the abundance of ice in these trenches. Our technique differs from previous efforts by taking advantage of the difference in reflective properties between ice rich soil and desiccated soil to derive Martian regolith optical constants directly from the Phoenix Surface Stereo Imager (SSI) data. We then used those optical constants to generate spectral mixture models to constrain the water-ice abundance in the icy soil. This reduces any assumptions as to what the regolith material is composed of, as the question we want to answer concerns the abundance of water-ice within that regolith, which in-turn offers insight into its emplacement.

Following this introduction is Section 2: a short review of the theory behind how we model spectra of mixtures as well as derive the necessary optical constants. In Section 3 we detail our methodology in applying these techniques to samples in the lab, as well as the results of these experiments. We then apply the methodology to data from the Phoenix Mars lander in Section 4. We discuss the results of that analysis and implications in Section 5 before our concluding remarks in Section 6.

2 Theory

The strong optical constants of most geologic materials in the visible-to-near-infrared (VNIR), and the resulting high reflectance values, result in a significant contribution of multiple scattering to the spectrum of an intimate mixture. Radiative transfer techniques (e.g. [Hapke, 2012, Shkuratov *et al.*, 1999]) are needed to model the spectrum of intimately mixed particles. We use the method of [Shkuratov *et al.*, 1999] to model the observed spectra. This method likens transmission, reflection, and scattering of light between mineral grains to that of propagating through a semi-infinite series of slab layers. Modeling of the mixture's spectrum requires a knowledge of the mixture's porosity and of each component's concentrations, grain sizes, and optical constants. These properties are encompassed by the one-dimensional scattering indicatrix for a layer, ρ_b (backwards) and ρ_f (forwards), and yield the albedo A [Shkuratov *et al.*, 1999]:

$$A = \frac{1 + \rho_b^2 - \rho_f^2}{2\rho_b} - \sqrt{\left(\frac{1 + \rho_b^2 - \rho_f^2}{2\rho_b}\right)^2 - 1} \tag{1}$$

The method of [Shkuratov *et al.*, 1999] models a one-dimensional albedo. [Shkuratov & Grynko, 2005] expand upon this model and provide a relationship between the bi-directional reflectance at a phase angle of 30° ($R(30°)$) and the one-dimensional albedo (A_{int}):

$$\log_{10}(R(30°)) = 1.088 \log_{10}(A_{int}) \tag{2}$$

JSC Mars-1 (g)	H_2O ice (g)	wt% ice	vol% ice
5.088	0.0	0.0	0.0
5.055	0.327	6.08	11.9
5.064	0.629	11.1	20.6
4.937	1.439	22.6	37.8

Table 1: Water-ice fraction of each of our sample mixtures.

While relationships for other viewing geometries can be derived [Shkuratov & Grynko, 2005], we constrained our laboratory work to a viewing geometry of 30° incidence and 0° emission since this relationship is already known. This viewing geometry is also less prone to background scatter we observed at greater phase angles.

Our primary motivation to utilize [Shkuratov *et al.*, 1999] over other spectral mixture models is that it is invertible, meaning we can compute optical constants of a material given its reflectance, porosity, and grain size S. This method requires the assumption of a real index of refraction and generates only the imaginary index of refraction k at a specific wavelength λ_i:

$$k(\lambda_i) = -\frac{\lambda_i}{4\pi S} \ln\left[\frac{b}{a} + \sqrt{\left(\frac{b}{a}\right)^2 - \frac{c}{a}}\right] \tag{3}$$

where a, b, and c encompass properties such as grain size and real index of refraction.

Subsequently, Kramers-Kronig analysis is used to find the index of refraction n at a specific wavelength λ_i by integrating over the imaginary index of refraction over all wavelengths:

$$n(\lambda_i) = n_{vis} + \frac{2(\lambda_{vis}^2 - \lambda_i^2)}{\pi} P \int_0^\infty \frac{\lambda^2 k(\lambda)}{(\lambda_i^2 - \lambda^2)(\lambda_{vis}^2 - \lambda^2)} d(\ln \lambda) \tag{4}$$

where P denotes the Cauchy principal part of the integral [Ahrenkiel, 1971, Dalton & Pitman, 2012]. We use equations 3 and 4 iteratively to converge on the optical constants of a material. However, subtractive Kramers-Kronig still assumes we know the real index of refraction at one wavelength λ_{vis}, so we estimate between a range (1.4-1.7) that is typical at 550 nm. We do not need to accurately extrapolate the spectrum from beyond our spectral range as subtractive Kramers-Kronig converges quickly [Ahrenkiel, 1971]. It is sufficient to assume a constant $k(\lambda)$ outside our spectral range.

3 Laboratory Methodology and Results

In order to determine the uncertainty of the methods discussed above, we tested them on mixtures of JSC Mars-1 (a Martian soil simulant [Allen *et al.*, 1998]) and water ice grains. These mixtures contained known concentrations of the two components (Table 1). We produced water-ice grains by grinding water-ice in a mortar and pestle within a freezer at about -20° C. Still within the -20° C freezer, we sieved both components to a size-range of 150-250 μm and measured the mass of each portion of the mixture before mixing carefully and thoroughly with a small spoon. In order to transform between wt.% and vol.%, we assumed mean particle densities of 1.91 g cm^{-3} [Allen *et al.*, 1998] and 0.9167 g cm^{-3} [Lide, 2005] for JSC Mars-1 and water ice, respectively.

As Shkuratov and Grynko provide Equation 2 for converting from a bidirectional reflectance with a phase angle of 30° to integral albedo [Shkuratov & Grynko, 2005], we set up our experiment such that light was incident at 30° and our spectrometer measured light emergent at 0°. Samples were measured on an adjustable stand, which ensured that both our white reference and our samples were measured at the same distance from the spectrometer.

After we measured spectra of a mixture sample, we needed to desiccate the sample. We were unable to place our samples in a Mars-like environment in order to sublimate the water ice, and placing the sample in a vacuum chamber at room temperature led to the water ice violently boiling and creating a rough surface texture. Instead, we placed the sample under a heat lamp to remove the ice via melting and evaporation. Once the sample was desiccated, we measured its spectrum again. All spectral measurements were performed at -20 °C using an Analytic Spectral Devices, Inc. (ASD) FieldSpec 3 spectrometer, and reflectance was reported relative to our Spectralon white reference. For each sample, we acquired 25 spectra at each of 5 points on the sample

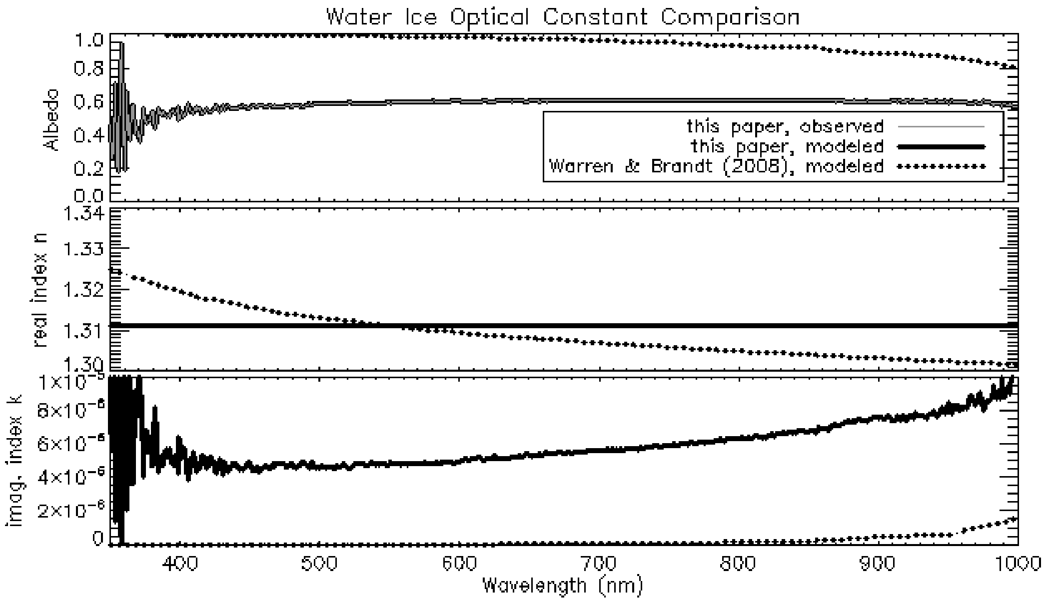

Figure 1: Top: Observed and modeled albedos of water ice grains. This paper's model uses the optical constants derived from the observed albedo, and hence our model perfectly overlies the observed albedo. Assumed ice grain particle size is irrelevant as long as the same size is assumed for the derivation of the optical constants as for the generation of the model spectra (in this case 200 μm). The other model uses optical constants from [Warren & Brandt, 2008]. Middle: Real index of refraction that we derived for water ice versus values from [Warren & Brandt, 2008]. Note that while there is a difference in slope, the absolute difference in $n(\lambda)$ between our optical constants and [Warren & Brandt, 2008]'s is less than 1%. Bottom: Imaginary index of refraction that we derived for water ice versus values from [Warren & Brandt, 2008].

to account for any inhomogeneous mixing across the sample. We calibrated the spectrometer for white reference and dark current before we took each set of spectra. We averaged all 125 spectra for each sample before and after desiccation.

We then used the spectra of desiccated soil to derive its optical constants using equations 3 and 4 . These equations assumed a knowledge of each endmember component's grain sizes, porosity, and the real index of refraction at an arbitrary wavelength.

Because the [Shkuratov *et al.*, 1999] method is invertible, as long as we assumed the same regolith grain size in deriving the optical constants as we did in modeling the regolith in a mixture we will achieve the same modeled results (Fig. 1).

We cannot ground-truth the water-ice grain sizes with Phoenix's suite of instruments, however the effect of water-ice grain size on the model spectrum throughout the Phoenix SSI spectral range (450-1000 nm) only becomes significant for ice grain sizes exceeding 1 mm (Fig. 2).

As noted in [Poulet *et al.*, 2002]'s comparison of [Shkuratov *et al.*, 1999] and [Hapke, 1981] spectral mixture theories, there is only a weak dependence of porosity on model spectra produced by the Shkuratov et al. method. For instance, modeling a 50/50 mixture of JSC Mars-1 and water-ice produces only a 3-6% increase in albedo with a decrease in porosity from 50 to 25 vol.% (Figure 3), approximately the range of porosities expected on Mars.

We derived our own optical constants for water ice using a sample of pure ice grains (Fig. 1). We assumed the real index of refraction of water-ice to be n=1.311 at 550 nm as per [Warren & Brandt, 2008].

Johnson and Grundy (2001) found JSC Mars-1 to have a real index of refraction $n = 1.56084 - 0.052355\lambda/\mu\text{m}$ [Johnson & Grundy, 2001]. Given that we would not have this information when deriving the optical constants of Martian regolith observed *in situ*, we modeled JSC Mars-1 with test values of n ranging from 1.4 to 1.7 at 550 nm. This range brackets the index of refraction of most common minerals [Guinness *et al.*, 1997].

We compare spectra of our icy soils (Table 1) to models generated using the optical con-

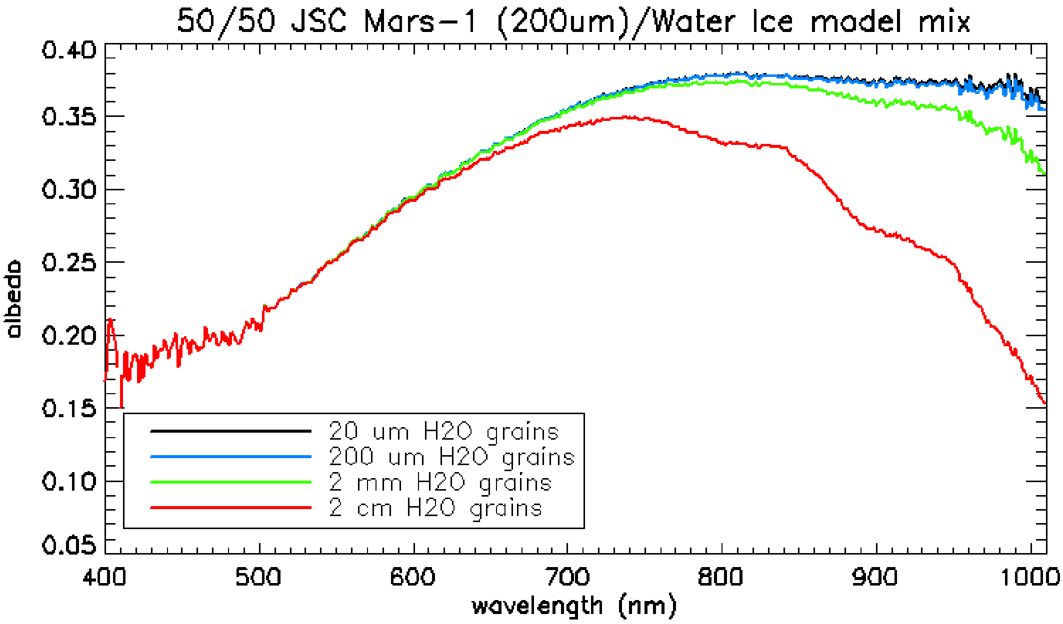

Figure 2: (Color) Modeled spectra of a mixture of JSC Mars-1 and water-ice for a range of water-ice grain sizes. The difference in spectra between water-ice at 20 and 200 μm is insignificant within the spectral range of interest. Significant effects on the spectra in the spectral region of interest only start occurring for grain sizes greater than 1 mm.

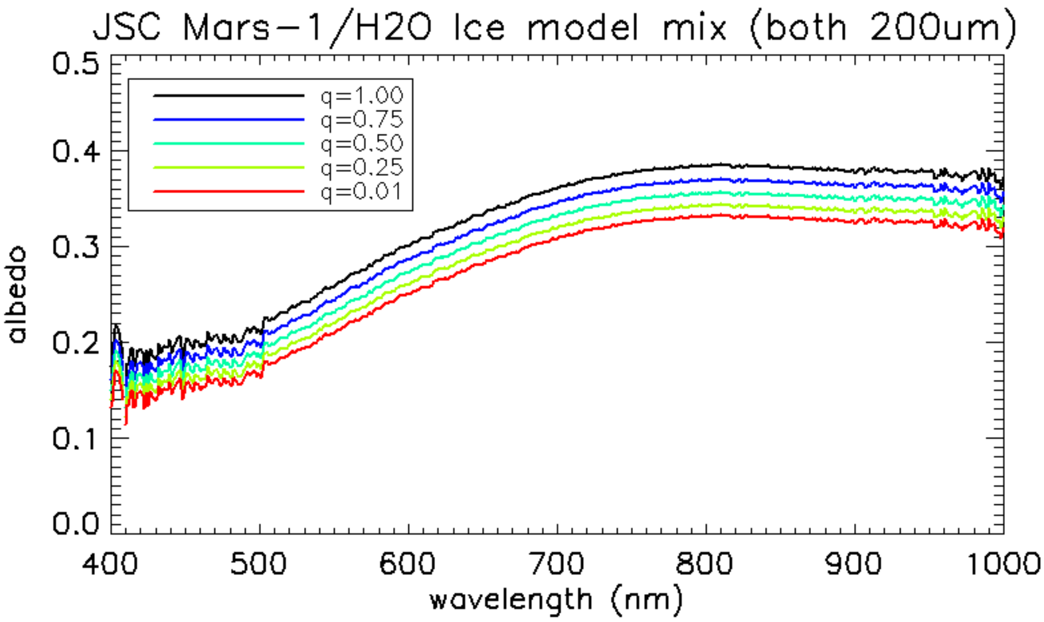

Figure 3: (Color) Modeled spectra of a mixture of 50 vol.% JSC Mars-1 and 50 vol.% water-ice (both with a grain size of 200 μm), assuming a range of porosities.

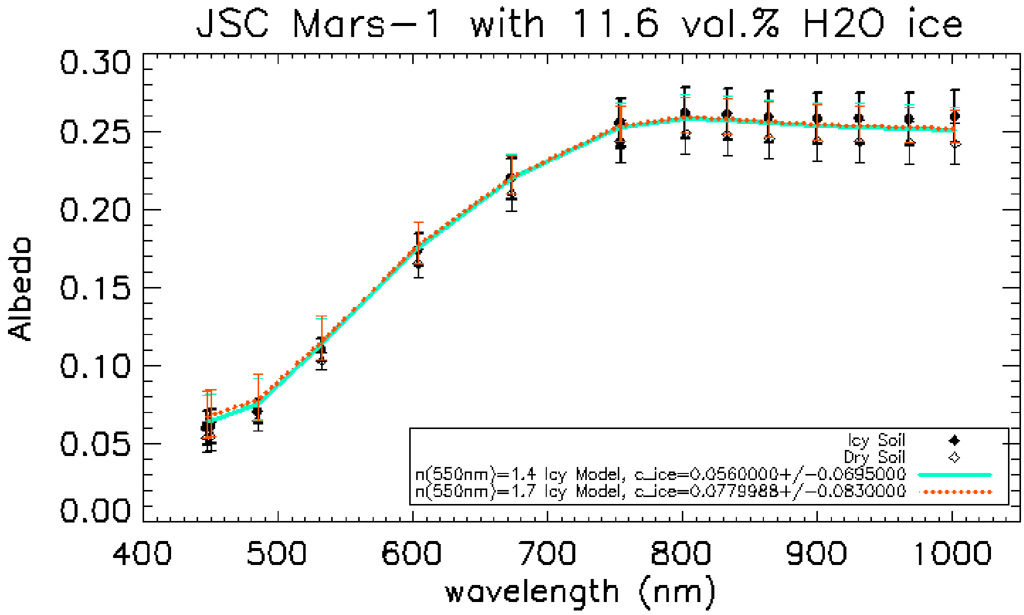

Figure 4: (Color) Reflectance spectrum of a mixture of 11.9 vol.% water-ice with JSC Mars-1 (solid black circles, thick error bars) and after desiccation (empty black circles, thin error bars), resampled to Phoenix SSI bandpasses. We use the standard deviation for our uncertainty. A solid blue line is our best fit model for the icy regolith assuming the real index of refraction n at 550nm was 1.4, while the orange dashed line assumes n(550nm)=1.7. The thin blue and orange error bars represent the best fit models at the extent of our uncertainties assuming n(550 nm)=1.4 and 1.7, respectively.

stants we derived for that sample's soil after water-ice has been removed. For water-ice we also use optical constants that we derived separately (due to the temperature dependence of the refractive index of ice). As we sieved both JSC Mars-1 and water-ice for grains between 150-250 μm, we assumed a grain size of 200 μm for both. We assume a volume fill fraction of 0.85; however porosity has little effect on model spectra.

We further constrained the uncertainty with which we can estimate the water-ice fraction of Martian regolith using Phoenix SSI by convolving our laboratory spectra with SSI's bandpass filters. We use the center wavelength and bandpass widths of [Lemmon *et al.*, 2008] with a filter transmission function provided by [Lemmon (Personal Communication)]:

$$T(\lambda) = e^{-\left(1.78\frac{\lambda-\lambda_C}{W}\right)^4} \tag{5}$$

where λ is wavelength, λ_C is the center wavelength of a bandpass, and W is bandpass width. Figures 4, 5, and 6 show our observed and modeled spectra convolved with SSI filter responses.

All other factors held constant, we fit for the concentration of water-ice grains iteratively and compare to the known original ice fraction (Table 2). In addition to the mean fit, we also fit our model to the mean albedo plus-or-minus the albedo's standard deviation. In terms of absolute volume percent, our mean model fit underestimates the actual water-ice by up to half, depending on the mixture. However, spectral models using the actual water-ice fraction fall within the 1σ envelope defined by the spectral models derived from average albedo plus-or-minus the standard deviation. Unknown values of porosity and real index of refraction at 500 nm will contribute to the uncertainty but the uncertainty is dominated by the standard deviation of our observed reflectances.

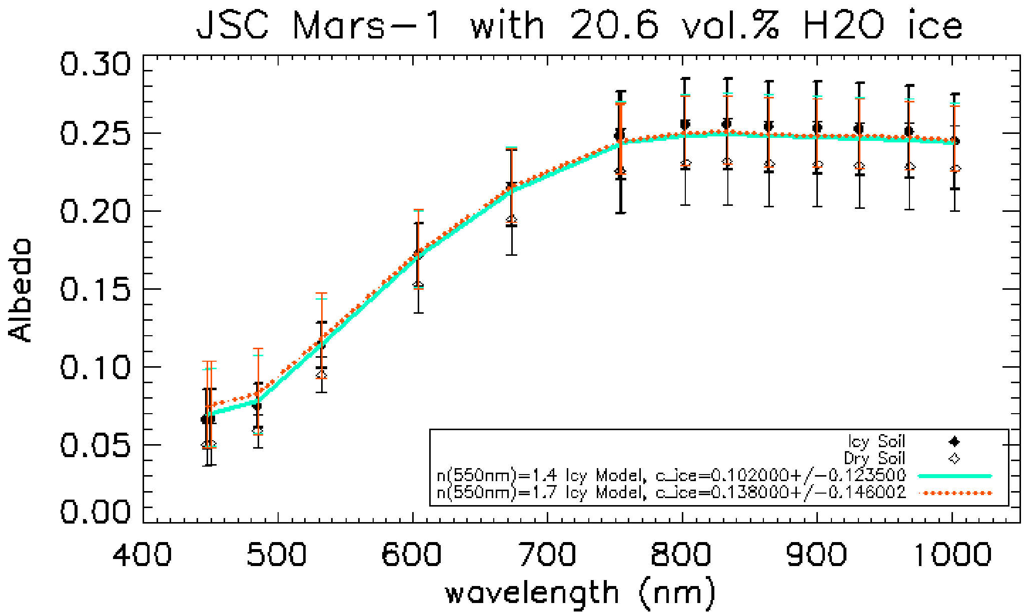

Figure 5: (Color) Reflectance spectrum of a mixture of 20.6 water-ice with JSC Mars-1 (solid black circles, thick error bars) and after dessication (empty black circles, thin error bars), resampled to Phoenix SSI bandpasses. We use the standard deviation for our uncertainty. A solid blue line is our best fit model for the icy regolith assuming the real index of refraction n at 550nm was 1.4, while the orange dashed line assumes n(550 nm)=1.7. The thin blue and orange error bars represent the best fit models at the extent of our uncertainties assuming n(550 nm)=1.4 and 1.7, respectively.

Ice Fraction		Best Fit (vol.%)	
vol.% ice	wt.% ice	n(550nm)=1.4	n(550nm)=1.7
11.9	6.08	6±7	8±8
20.6	11.1	10±12	14±15
37.8	22.6	25±17	30±19

Table 2: Water-ice fraction of each of our sample mixtures, both known values and best fit values.

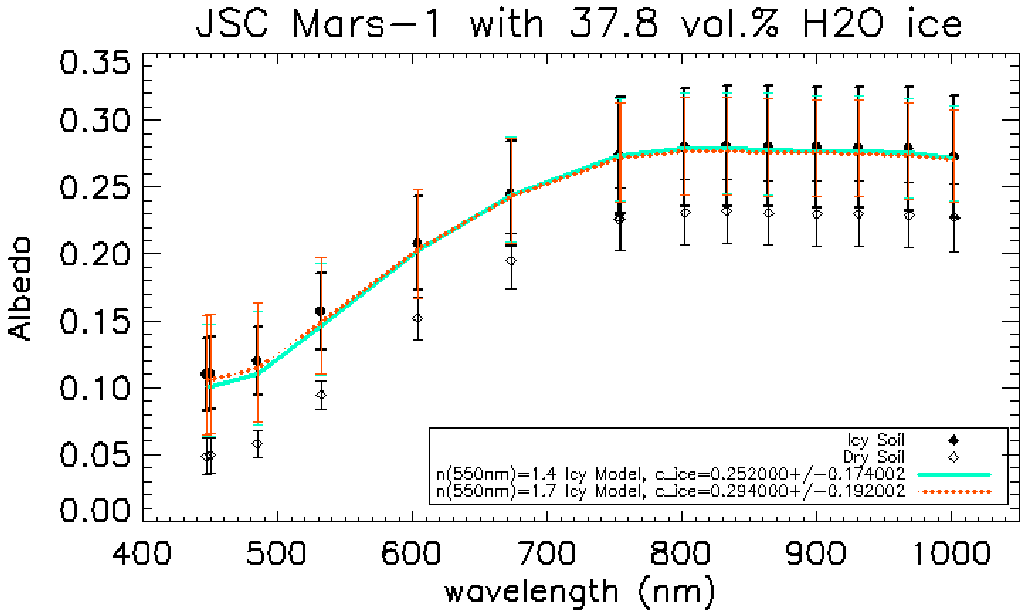

Figure 6: (Color) Reflectance spectrum of a mixture of 37.8 water-ice with JSC Mars-1 (solid black circles, thick error bars) and after dessication (empty black circles, thin error bars), resampled to Phoenix SSI bandpasses. We use the standard deviation for our uncertainty. A solid blue line is our best fit model for the icy regolith assuming the real index of refraction n at 550nm was 1.4, while the orange dashed line assumes $n(550\text{ nm})=1.7$. The thin blue and orange error bars represent the best fit models at the extent of our uncertainties assuming $n(550\text{ nm})=1.4$ and 1.7, respectively.

4 Application to Phoenix Data

4.1 Snow White Trench

Phoenix excavated Snow White Trench (Figure 7) to find water-ice mixed with the regolith. By Sol 45 (Figure 8), the same bright icy material appeared darker than the surrounding soil because the ice is forward-scattering [Cull *et al.*, 2010] (see viewing geometries in table 3). On Sol 50, the water-ice had sublimated completely, such that the spectrum of the soil which used to contain water-ice matched the surrounding soil (Figure 9). Because these two spectra matched, we used the spectrum of the non-icy regolith aquired on Sol 43 to derive optical constants.

We used SSI I/F (IOF) images where I is radiance from the scene, and πF is radiance from the Sun at the Martian surface, corrected for Sun angle (such that the light is incident perpendicular to the surface), atmospheric opacity, and dust [Drube *et al.*, 2010]. Light reflected by Snow White Trench to SSI was at an emergent angle of approximately 47°, and not at 30° for which we could use Equation 2. While Shkuratov and Grynko did not provide a relation between bidirectional reflectance at a 47° phase angle and integral albedo, we derived a relation for reflectance at 50° phase to integral albedo from a plot of this relationship in their paper [Shkuratov & Grynko, 2005]:

$$\log_{10}(R(50°)) = 1.013\log_{10}(A_{int}) \qquad (6)$$

Were the equation truly for a phase angle of 47°, we would expect a constant between 1.013 and 1.088 (Equations 6 and 2, respectively), but closer to 1.013. Nevertheless, we used equation 6 to transform SSI reflectance spectra into the integral albedo spectra used in the Shkuratov et al. methodology [Shkuratov *et al.*, 1999].

To derive the regolith's optical constants, we assumed a grain size of 60 μm [Goetz *et al.*, 2010] and a porosity of 0.5 (for the dessicated regolith, following [Zent *et al.*, 2010]'s porosity measurement of 50-55% in the upper 15 mm of the Martian surface). Since the porosity range of dry regolith is only 5 vol.%, modeled albedo is not expected to vary by more than 1%. Ice grain size matters

Trench Observed	Sol	i	e	ψ	PDS Product ID	Activity
Snow White	43	64°	48°	191°	ss043rad900005586_14b04l1m1 etc.	14b0
	45	56°	45°	2°	ss045rad900218012_15030l1m1 etc.	1503
	50	56°	40°	5°	ss050rad900661943_159b0l1m1 etc.	159b
Dodo-Goldilocks	24	56°	46°	76°	ss024rad898354633_12e50l1m1 etc.	12e5

Table 3: Viewing geometries of Phoenix Lander trench observations used in this study, where i is the incidence angle of light upon the trench (90° - solar elevation angle), e is the emergence angle of light from the trench (90° - SSI elevation angle), and ψ is the azimuthal angle between the Sun and SSI. The IOF observations we used normalized incidence to $i = 0$. Note that although the three Snow White trench observations had different e, this is for the center of the image. Observations on Sol 43 and 45 were centered upon the trench, while the Sol 50 observation was centered on the near-side trench wall. For reference, we include the Planetary Data System (PDS) product ID of the first image in each set of SSI images we used for our analysis, and the activity under which these image products fall.

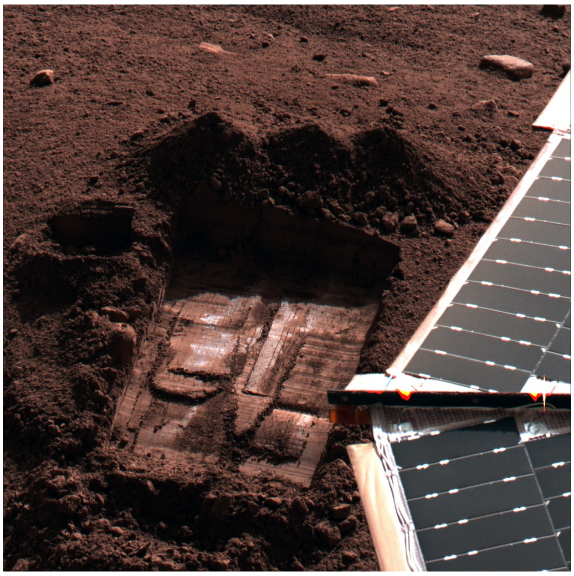

Figure 7: (Color) SSI color image (RGB = SSI Filters RA, RB, RC) of Snow White Trench on Sol 43, from activity 14b0 (*e.g.* PDS product ID ss043rad900005586_14b04l1m1). TEGA analysis confirms the bright portion of the trench contains water ice [Smith *et al.*, 2009].

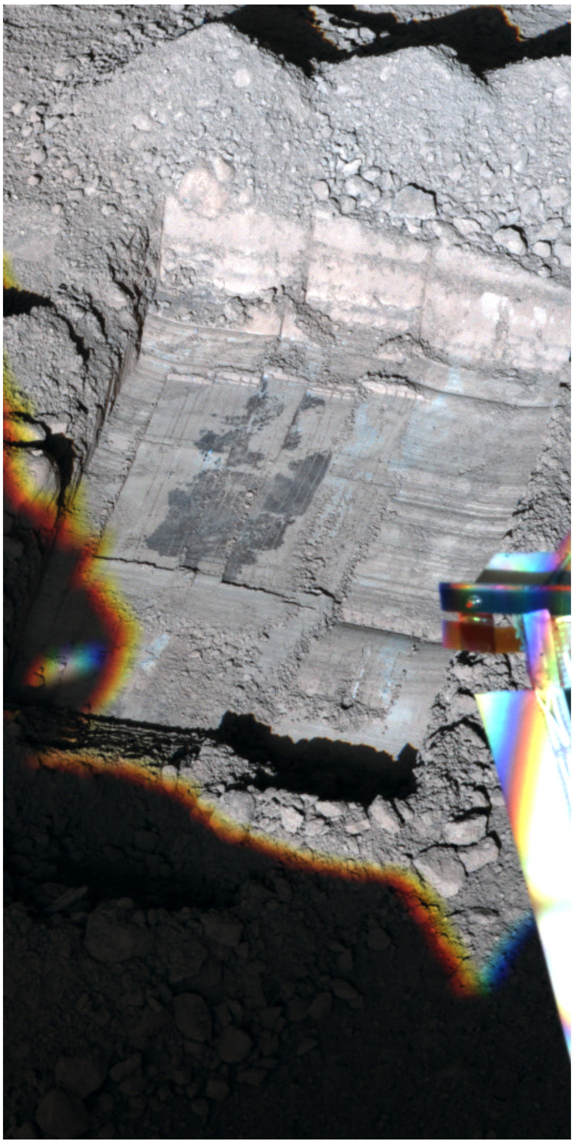

Figure 8: (Color) SSI color image (RGB = SSI Filters RA, RB, RC) of Snow White Trench on Sol 45, from activity 1503 (*e.g.* PDS product ID ss045rad900218012_15030l1m1). The dark material at the bottom of the trench is the bright material from Figure 7.

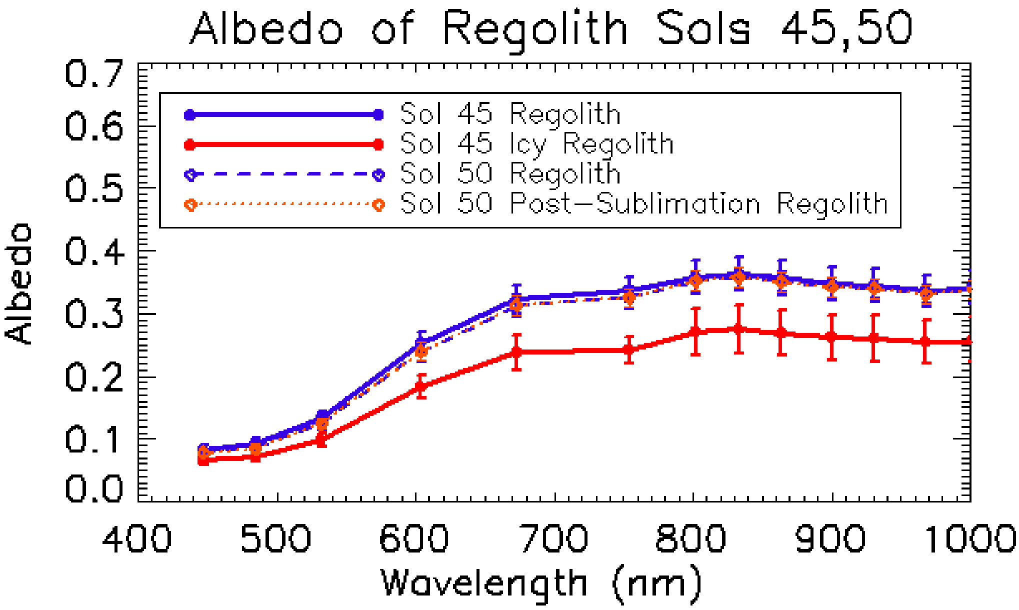

Figure 9: (Color) The spectrum of regolith after ice sublimation from Sol 45 to 50 (solid red line to dotted orange line) matches the spectra of the non-icy regolith both before (Sol 45, solid blue line) and after (Sol 50, dashed blue line) the icy in the regolith beside it has sublimated.

very little until beyond the wavelength range of Sol 43 observations (Fig. 2), so we also assumed 60 μm ice grain size for simplicity. We used water-ice optical constants from [Warren & Brandt, 2008] for our models, as we could not independently measure the water-ice optical constants like we did in the lab. This left our greatest uncertainty to be the real index of refraction of the Martian regolith at 550 nm, so we estimated a value between n=1.4 to n=1.7 (Fig. 10) as we did for our experiments with JSC Mars-1. Holding all other values constant, we found a best-fit model varying water-ice concentration. Depending on our assumed real index of refraction at 550 nm, our models fit best for 24-27 vol.% water-ice within the icy regolith exposed at Snow White Trench. We also fit models to the mean albedo with the addition or subtraction of its standard deviation, and found the best-fit water-ice concentration varies up to 12 vol.%.

4.2 Dodo-Goldilocks Trench

Phoenix excavated Dodo-Goldilocks trench (Figure 12) on Sol 24 to expose bright water-ice. Dodo-Goldilocks was viewed at an emergent angle of 44°, so we again used equation 6 to convert from IOF bidirectional reflectance to integral albedo before applying our model. As was the case with Snow White Trench, we expect the conversion coefficient to be between those of Equations 2 and 6, but still closer to that of the latter. We again assumed regolith grain-size of 60 μm, with optical constants derived from non-icy soil observed on Sol 24. These optical constants are similar to those derived for the regolith on Sol 43 at the Snow White Trench (Figure 11), differing most at wavelengths where their albedos also differed.

Only large water-ice grains (relative to regolith grain size) can explain the observed drop in reflectance in the near-infrared of the icy soil spectrum (Figure 2), as this feature does not appear in the dessicated regolith spectrum (Figure 13). Indeed, when we fit for water-ice grain size and concentration with a least-squares method we find an ice grain size of 1.0-1.3 mm, with an abundance of 85-87 vol.% depending on whether we assumed n(550 nm)=1.4 or 1.7. As with the Snow White Trench, we also fit our model to the extents of the uncertainty in the albedo, finding concentration uncertainty of $\pm$5 vol.% and grain size uncertainty of $\pm$0.4 mm.

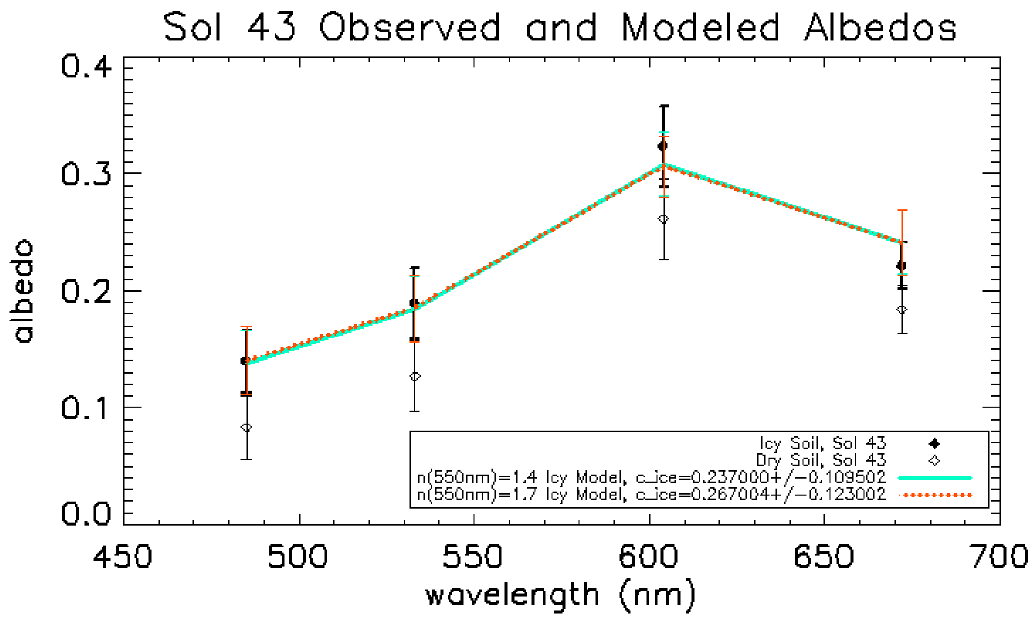

Figure 10: (Color) Reflectance spectra of the icy (solid black circles, thick error bars) and dry (empty black circles, thin error bars) regoliths. Best-fit modeled albedo spectra of mixtures of non-icy regolith with water-ice, assuming both regolith (optical constants derived from the non-icy regolith) and water-ice grains to be 60 μm, an initial volume-fill fraction without water-ice of 0.5, and the regolith's real-index of refraction at 550 nm to vary from 1.4 (solid blue line) to 1.7 (orange dashed line). The thin blue and orange error bars represent the best fit models at the extent of our uncertainties assuming n(550 nm)=1.4 and 1.7, respectively.

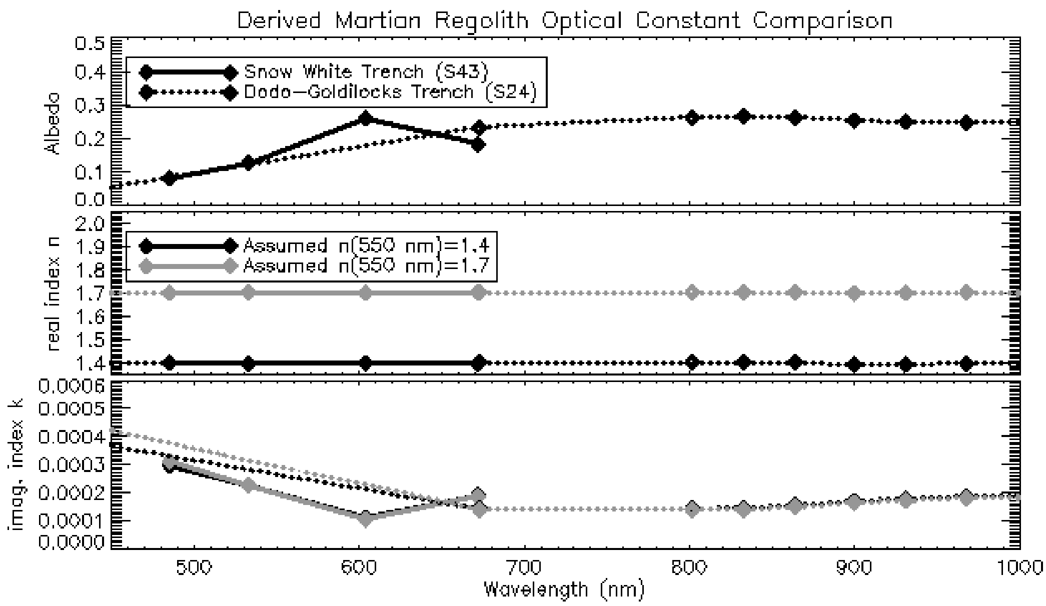

Figure 11: Top: Observed albedos of the Martian regolith in both the Snow White Trench (solid) and Dodo-Goldilocks Trench (dotted). Middle: Real index of refraction derived for the regolith at each site, assuming either that the real index of refraction is 1.4 (black) or 1.7 (grey) at 550 nm. Bottom: Imaginary index of refraction derived for the regolith at each site.

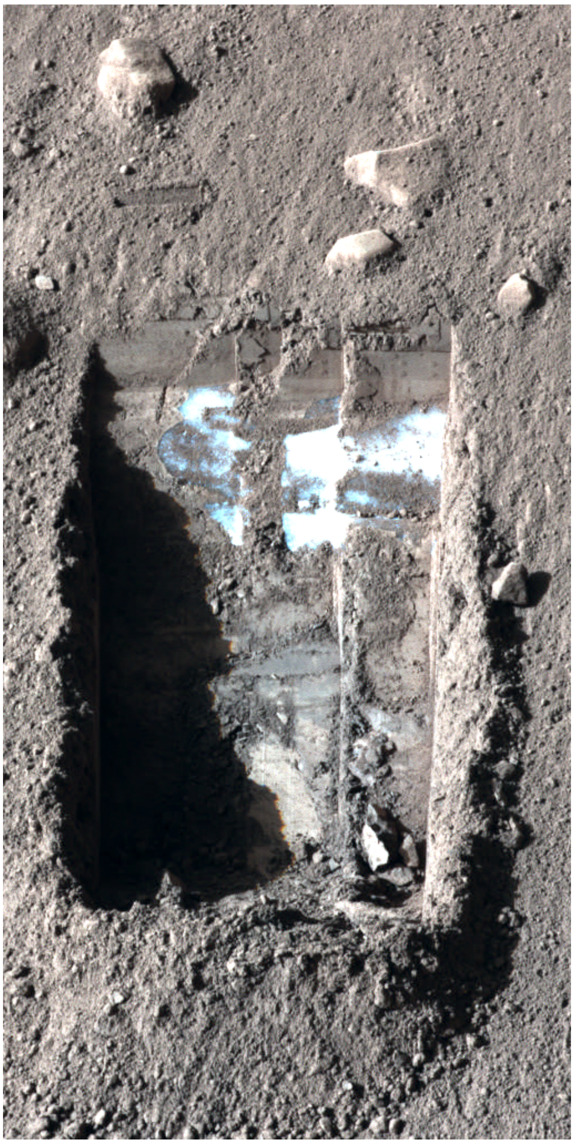

Figure 12: (Color) SSI color image (RGB = SSI Filters RA, RB, RC) of Dodo-Goldilocks Trench on Sol 24, from activity 12e5 (*e.g.* PDS product ID ss024rad898354633_12e50l1m1).

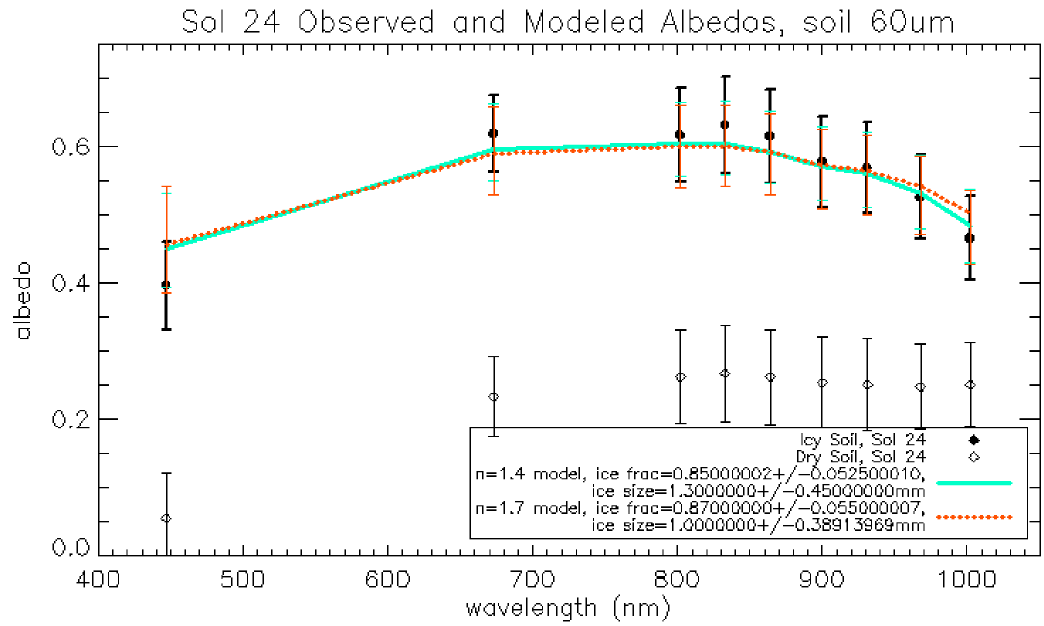

Figure 13: (Color) Observations of ice reflectance (solid black circles, thick error bars) and Martian regolith reflectance (empty black circle, thin error bars) in the Dodo-Goldilocks Trench on Sol 24. Regolith grains are assumed to be 60 μm, with optical constants derived from the non-icy regolith. Best-fit modeled albedo spectra of mixtures of non-icy regolith with water-ice vary the regolith's real-index of refraction at 550 nm to from 1.4 (solid blue line) to 1.7 (orange dashed line). The thin blue and orange error bars represent the best fit models at the extent of our uncertainties assuming $n(550\text{ nm})=1.4$ and 1.7, respectively. Water-ice grain size was allowed to vary.

5 Discussion

Our analysis found Snow White Trench to have 24-27±12 vol.% water-ice. Assuming the same densities as we did in our laboratory experiments [Allen *et al.*, 1998, Lide, 2005], this translates into 14-15±7 wt.%. In our laboratory experiments, the actual water-ice fraction tended to be greater than the best-fit water-ice fraction, but was still within the uncertainty. This water-ice fraction is consistent with emplacement by vapor diffusion, wherein water-ice forms within the pore spaces of the Martian regolith, depositing from the atmosphere [Mellon *et al.*, 2004, Hudson *et al.*, 2009, Siegler *et al.*, 2012]. This emplacement mechanism guarantees that ice grains are evenly mixed within the regolith. [Mellon *et al.*, 2009] also concluded that Snow White Trench and similar trenches were the result of vapor diffusion, further citing that present atmospheric conditions enable vapor diffusion and that the soil did not collapse with the sublimation of water-ice. [Cull *et al.*, 2010] used the methods within [Hapke, 2012] to model mixtures of water ice and palagonite [Clancy *et al.*, 1995] in order to estimate the water-ice fraction of Snow White Trench, finding 30±20 wt.% water-ice, or $\sim 53 \pm 29$ vol.% water-ice. Our results are broadly consistent with [Cull *et al.*, 2010]'s.

Our models indicated that Dodo-Goldilocks Trench contains 85-87±6 vol.% water-ice, exceeding the estimated 50-55 vol.% porosity of Martian regolith [Zent *et al.*, 2010]. These results led to our conclusion that the Dodo-Goldilocks trench must be largely ice, as the ice is far greater than pore-filling. [Cull *et al.*, 2010] also modeled Dodo-Goldilocks and found that Dodo-Goldilocks Trench was >99 wt.% water-ice. While the water-ice fraction estimates between our studies differ, they both concluded that the ice in Dodo-Goldilocks Trench far exceeded pore-filling [Cull *et al.*, 2010]. Alternate emplacement mechanisms include freezing of water in wet soil, or the formation of ice lenses or needles [Smith *et al.*, 2009].

By choosing to use the [Shkuratov *et al.*, 1999] model for its analytic inversion to solve for optical constants, we sacrificed the angular dependence given in other radiative transfer models (e.g. [Hapke, 1981]). This became problematic for Snow White Trench as ice grains could either brighten or darken a surface depending on the azimuthal angle between the observer and the Sun, whereas our mixture model only brightened with ice grains. For observation conditions similar to $i = 0°$ and $e = 30 - 50°$, [Shkuratov *et al.*, 1999, Shkuratov & Grynko, 2005] worked well, but other models may work better at other geometries. Regardless of the exact methods of deriving regolith optical constants or modeling spectra of ice-regolith mixtures, our technique still eliminates the need to know or assume what the regolith is made of in determining its water-ice content.

Ultimately, this technique will prove useful aboard future missions to the Martian permafrost, in that we can determine water-ice content of the surrounding regolith using only cameras—allowing smaller and cheaper spacecraft to still do this science. The methodology can also be adopted in other locales such as the permanently shadowed regions of the Moon. Future instruments may also consider examining regolith with filters in the 1.5 or 2.0 μm wavelength regions where water-ice absorption features are located. These methods might also find themselves useful examining ices of other volatiles on future landers visiting moons or other small bodies in the outer solar system.

6 Conclusions

Our laboratory experiments demonstrate our technique's ability to estimate the abundance of water ice in ice-soil mixtures (with soil optical constants derived from the spectrum of the soil alone) to within the 1σ envelope defined by fitting mixture models to the observed albedo spectrum plus-or-minus uncertainty. This uncertainty was dominated by the uncertainty of the observed albedo itself. We applied this procedure to data from Phoenix lander SSI as an exercise and found Snow-White-trench ice to be pore-filling and Dodo-Goldilocks-trench ice to be relatively-pure ice, agreeing with the results of [Cull *et al.*, 2010, Smith *et al.*, 2009]. However, unlike the prior studies we did not need to assume regolith composition, and that offers a boon in determining water-ice content of regoliths for which we may not have exact analogues or optical constants for.

7 Acknowledgements

We are grateful for insights from Mark Lemmon and Ted Roush, and for comments from anonymous reviewers. Szilárd Gyalay and Kathryn Chu were funded for this work by internships through NASA USRA.

References

[Ahrenkiel, 1971] Ahrenkiel, R.K. (1971). "Modified Kramers-Kronig analysis of optical spectra." *Journal of he Optical Society of America 61*(12), 1651-1655. doi: 10.1364/JOSA.61.001651

[Allen *et al.*, 1998] Allen, C.C., R.V. Morris, K.M. Jager, D.C. Golden, D.J. Lindstrom, M.M. Lindstrom, J.P. Lockwood (1998). "Martian Regolith Simulant JSC Mars-1." *Lunar and Planetary Science Conference XXIX*, abstract 1690.

[Boynton *et al.*, 2002] Boynton, W.V., W.C. Feldman, S.W. Squyres, T.H. Prettyman, J. Brückner, L.G. Evans, R.C. Reedy, R. Starr, J.R. Arnold, D.M. Drake, P.A.J. Englert (2002). "Distributon of hydrogen in the near surface of Mars: Evidence for subsurface ice depositys." *Science 297*(5578), 81-85.

[Carr *et al.*, 1990] Carr, M.C. (1990). "D/H on Mars: Effects of floods, volcanism, impacts, and polar processes." *Icarus 87*(1), 210-227. doi: 10.1016/0019-1035(90)90031-4

[Clancy *et al.*, 1995] Clancy, R.T., S.W. Lee, G.R. Gladstone, W.W. McMillan, T. Rousch (1995). "A new model for Mars atmospheric dust based upon analysis of ultraviolet through infrared observations from Mariner 9, Viking, and Phobos." *Journal of Geophysical Research: Planets 100*(E3), 5251-5263.

[Cull *et al.*, 2010] Cull, S., R.E. Arvidson, M.T. Mellon, P. Skemer, A. Shaw, R.V. Morris (2010). "Compositions of subsurface ices at the Mars Phoenix landing site." *Geophysical Research Letters 37*(24). doi: 10.1029/2010GL045372

[Dalton & Pitman, 2012] Dalton III, J.B. & K.M. Pitaman (2012). "Low temperature optical constants of some hydrated sulfates relevant to planetary surfaces." *Journal of Geophysical Research 117*. doi: 10.1029/2011JE004036

[Diez *et al.*, 2008] Diez, B., W.C. Feldman, S. Maurice, O. Gasnault, T.H. Prettyman, M.T. Mellon, O. Aharonson, N. Schorghofer (2008). "H Layering in the top meter of Mars." *Icarus 196*(2), 409-421. doi: 10.1016/j.icarus.2008.02.006

[Dundas *et al.*, 2014] Dundas, C.M., S. Byrne, A.S. McEwen, M.T. Mellon, M.R. Kennedy, I.J. Daubar, L. Saper (2014). "HiRISE observations of new impact craters exposing Martian ground ice." *Journal of Geophysical Research: Planets 119*(1), 109-127.

[Dundas *et al.*, 2018] Dundas C.M., A.M. Bramson, L. Ojha, J.J. Wray, M.T. Mellon, S. Byrne, A.S. McEwen, N.E. Putzig, D. Viola, S. Sutton, E. Clark (2018). Exposed subsurface ice sheets in the Martian mid-latitudes." *Science 359*(6372), 199-201.

[Drube *et al.*, 2010] Drube, L., K. Leer, W. Goetz, H. P. Gunnlaugsson, M. P. Haspang, N. Lauritsen, M. B. Madsen, L. K. D. Sørensen, M. D. Ellehoj, M. T. Lemmon, R. V. Morris, D. Blaney, R. O. Reynolds, P. H. Smith (2010). "Magnetic and optical properties of airborne dust and settling rates of dust at the Phoenix landing site." *Journal of Geophysical Research: Planets 115*(E5). doi: 10.1029/2009JE003419

[Goetz *et al.*, 2010] Goetz, W., W. T. Pike, S. F. Hviid, M. B. Madsen, R. V. Morris, M. H. Hecht, U. Staufer, K. Leer, H. Sykulska, E. Hemmig, J. Marshall, J. M. Morookian, D. Parrat, S. Vijendran, B. J. Bos, M. R. El Maarry, H. U. Keller, R. Kramm, W. J. Markiewicz, L. Drube, D. Blaney, R. E. Arvidson, J. F. Bell III, R. Reynolds, P. H. Smith, P. Woida, R. Woida, R. Tanner (2010). "Microscopy analysis of soils at the Phoenix landing site, Mars: Classification of soil particles and description of their optical and magnetic properties." *Journal of Geophysical Research 115*(E8). doi: 10.1029/2009JE003437

[Guinness *et al.*, 1997] Guinness, E.A, R.E. Arvidson, I.H.D. Clark, M.K. Shepard (1997). "Optical scattering properties of terrestrial varnished basalts compared with rocks and soils at the Viking Lander sites." *Journal of Geophysical Research 102*(E12), 28,687-28,703.

[Hapke, 1981] Hapke, B. (1981) "Bidirectional reflectance spectroscopy. I. Theory." *Journal of Geophysical Research 86*, 3039-3054.

[Hapke, 2012] Hapke, B. (2012) *Theory of Reflectance and Emittance Spectroscopy.* Cambridge University Press. 2nd. Edition.

[Hudson *et al.*, 2009] Hudson, T.L., O. Aharonson, N. Schorghofer (2009). "Laboratory experiments and models of diffusive emplacement of ground ice on Mars." *Journal of Geophysical Research: Planets 114*(E1). doi: 10.1029/2008JE003149

[Johnson & Grundy, 2001] Johnson, J.R., W.M. Grundy (2001). "Visible/near-infrared spectra and two-layer modeling of palagonite-coated basalts." *Geophysical Research Letters 28*(10), 2101-2104. doi: 10.1029/2000GL012669

[Konrad *et al.*, 1993] Konrad, J.M., C. Duquennoi (1993). "A model for water transport and ice lensing in freezing soils." *Water Resources Research 29*(9), 3109-3124. doi: 10.1029/93WR00773

[Lemmon *et al.*, 2008] Lemmon, M.T., P. Smith, C. Shinohara, R. Tanner, P. Woida, A. Shaw, J. Hughes, R. Reynolds, R. Woida, J. Penegor, C. Oquest, S.F. Hviid, M.B. Madsen, M. Olsen, K. Leer, L. Drube, R.V. Morris, D. Britt (2008). "The Phoenix Surface Stereo Imager (SSI) Investigation." *Lunar and Planetary Science Conference*, Abstract 2156.

[Lemmon (Personal Communication)] Lemmon, M. (2017 August 16) Personal Communication.

[Lide, 2005] Lide, D.R. (Ed., 2005). *CRC Handbook of Chemistry and Physics, 86th Edition Edited.*

[Mellon *et al.*, 2004] Mellon, M.T., W.C. Feldman, & T.H. Prettyman (2004). "The presence and stability of ground ice in the southern hemisphere of Mars." *Icarus 169*(2), 324-340. doi: 10.1016/j.icarus.2003.10.022

[Mellon *et al.*, 2008] Mellon, M.T., R.E. Arvidson, J.J. Marlow, R.J. Phillips, E. Asphaug (2008). "Periglacial landforms at the Phoenix landing site and the northern plains of Mars." *Journal of Geophysical Research: Planets*(E3).

[Mellon *et al.*, 2009] Mellon, M.T., R.E. Arvidson, H.G. Sizemore, M.L. Searls, D.L. Blaney, S. Cull, M.H. Hecht, T.L. Heet, H.U. Keller, M.T. Lemmon, W.J. Markiewicz, D.W. Ming, R.V. Morris, W.T. Pike, A.P. Zent (2009). "Ground ice at the Phoenix Landing Site: Stability state and origin." *Journal of Geophysical Research: Planets 114*(E1). doi: 10.1029/2009JE003417

[Mischna *et al.*, 2003] Mischna, M.A., M.I. Richardson, R.J. Wilson, D.J. McCleese (2003). "On the orbital forcing of Martian water and CO2 cycles: A general circulation model study with simplified volatile schemes." *Journal of Geophysical Research: Planets 108*(E6). doi: 10.1029/2003JE002051

[Moore *et al.*, 1987] Moore, H.J., R.E. Hutton, G.D. Clow, C.R. Spitzer (1987). *Physical properties of the surface materials at the Viking landing sites on Mars.* No. 1389.

[Noe Dobrea *et al.*, 2015] Noe Dobrea, E.Z., C.R. Stoker, C.P. McKay, A.F. Davila, M. Krčo (2015). "Crater Morphology in the Phoenix Landing Ellipse: Insights into Net Erosion and Ice Table Depth." *46th Lunar and Planetary Science Conference*, in The Woodlands, Texas. LPI Contribution No. 1832, p.2511.

[Noe Dobrea *et al.*, 2018] Noe Dobrea, E.Z. A.J. Dombard, C.R. Stoker, D.C. Berman D. C., A.F. Davila, and C.P. McKay (2018). "Ground-Ice and Viscous Relaxation of Craters at the Phoenix Landing Site." *Late Mars Workshop 2018* Abstract 50

[Plaut *et al.*, 2009] Plaut, J.J., A. Safaeinili, J.W. Holt, R.J. Phillips, J.W. Head III, R. Seu, N.E. Putzig, A. Frigeri (2009). "Radar evidence for ice in lobate debris aprons in the mid[U+2010]northern latitudes of Mars." *Geophysics Research Letters 36*(2), L02203. doi:10.1029/2008GL036379

[Poulet *et al.*, 2002] Poulet, F., J.N. Cuzzi, D.P. Cruikshank, T. Roush, C.M. Dalle Ore (2002). "Comparison between the Shkuratov and Hapke scattering theories for solid planetary surfaces: Application to the surface composition of two Centaurs." *Icaurs 160*(2), 313-324.

[Prettyman *et al.*, 2004] Prettyman, T.H., W. C. Feldman, M. T. Mellon, G. W. McKinney, W. V. Boynton, S. Karunatillake, D. J. Lawrence, S. Maurice, A. E. Metzger, J. R. Murphy, S. W. Squyres, R. D. Starr, R. L. Tokar (2004). "Composition and structure of the Martian surface at high southern latitudes from neutron spectroscopy." *Journal of Geophysical Research: Planets 109*(E5). doi: 10.1029/2003JE002139

[Putzig *et al.*, 2014] Putzig, N.E., R.J. Phillips, B.A. Campbell, M.T. Mellon, J.W. Holt, T.C. Brothers (2014) . "SHARAD soundings and surface roughness at past, present, and proposed landing sites on Mars: Reflections at Phoenix may be attributable to deep ground ice." *Journal of Geophysical Research: Planets 119*(8), 1936-1949. doi: 10.1002/2014JE004646

[Shkuratov *et al.*, 1999] Shkuratov, Y.G., L. Starukhina, H. Hoffmann, G. Arnold (1999). "A Model of Spectral Albedo of Particulate Surfaces: Implications for Optical Properties of the Moon." *Icarus 137*(2), 235-246. doi: 10.1006/icar.1998.6035

[Shkuratov & Grynko, 2005] Shkuratov, Y.G., Y.S. Grynko (2005). "Light scattering by media composed of semitransparent particles of different shapes in ray optics approximation: consequences for spectroscopy, photometry and polarimetry f planetary regoliths." *Icarus 173*(1), 16-28.

[Siegler *et al.*, 2012] Siegler, M., O. Aharonson, E. Carey, M. Choukroun, T. Hudson, N. Schorghofer, S. Xu (2012). "Measurements of thermal properties of icy Mars regolith analogs." *Journal of Geophysical Research: Planets 117*(E3). doi: 10.1029/2011JE003938

[Smith *et al.*, 2009] Smith, P.H., L. K. Tamppari, R. E. Arvidson, D. Bass, D. Blaney, W. V. Boynton, A. Carswell, D. C. Catling, B. C. Clark, T. Duck, E. DeJong, D. Fisher, W. Goetz, H. P. Gunnlaugsson, M. H. Hecht, V. Hipkin, J. Hoffman, S. F. Hviid, H. U. Keller, S. P. Kounaves, C. F. Lange, M. T. Lemmon, M. B. Madsen, W. J. Markiewicz, J. Marshall, C. P.

McKay, M. T. Mellon, D. W. Ming, R. V. Morris, W. T. Pike, N. Renno, U. Staufer, C. Stoker, P. Taylor, J. A. Whiteway, A. P. Zent (2009). "H_2O at the Phoenix Landing Site." *Science 325*(5936), 58-61. doi: science.1172339

[Warren & Brandt, 2008] Warren, S.G., R.E. Brandt (2008). "Optical constants of ice from the ultraviolet to the microwave: A revised compilation." *Journal of Geophysical Research: Atmospheres 113*(D4).

[Zent *et al.*, 2010] Zent, A.P., M.H. Hecht, D.R. Cobos, S.E. Wood, T.L. Hudson, S.M. Milkovich, L.P. DeFlores, M.T. Mellon (2010). "Initial results from the thermal and electrical conductivity probe (TECP) on Phoenix." *Journal of Geophysical Research: Planets 115*(E3).